JOURNAL OF GEOPHYSICAL RESEARCH, VOL. 100, NO. B4, PAGES 5941–5952, APRIL 10, 1995

Simple mathematical model of a rough fracture

Stephen R. Brown

Geomechanics Department, Sandia National Laboratories, Albuquerque, New Mexico

Abstract. A simple mathematical model of rough-walled fractures in rock is described which requires the specification of only three main parameters: the fractal dimension, the rms roughness at a reference length scale, and a length scale describing the degree of mismatch between the two fracture surfaces. Fractured samples, collected from natural joints and laboratory specimens, have been profiled to determine the range of these three parameters in nature. It is shown how this surface roughness model can be implemented on a computer, allowing future detailed study of the mechanical and transport properties of single fractures and the scale dependence of these properties.

Introduction

Fractures are well known for their effects on the mechanical and transport properties of rock. Mechanical properties, such as bulk elastic constants and shear strength, are strongly affected by the presence of fractures [*Goodman*, 1976; *Brown and Scholz*, 1986]. Fractures also control the hydraulic conductivity of crystalline and tight sedimentary rock [*Kranz et al.*, 1979; *Brace*, 1980]. These effects arise from the fact that the surfaces composing a fracture are rough and mismatched at some scale. The shape, size, and number of contacts between the surfaces control the mechanical properties. The surfaces are propped apart by the contacting asperities, and the resulting space between the surfaces (or aperture) controls the transport properties. Surface roughness is therefore important to quantify for the study of many fracture properties.

It is well established that the roughness of fracture surfaces in rock depends on the sample size or scale of observation [*Brown and Scholz*, 1985; *Power and Tullis*, 1991]. Furthermore, it is known that the two surfaces composing a fracture are often well matched or mated with one another above some particular length scale [*Brown et al.*, 1986]. Since many properties of a fracture depend on surface roughness, the scale dependence of roughness may result in a corresponding scale dependence of the mechanical and transport properties. It is important to understand these scaling laws in order to allow extrapolation of the results of laboratory measurements to the field.

To aid in future study of the dependence of the physical properties of fractures on surface roughness and specimen size, in this paper I present a simple mathematical model of a rough fracture. As will be seen, this model requires the specification of only three main parameters: the fractal dimension, the rms roughness at a reference length scale, and a length scale describing the degree of mismatch between the two fracture surfaces. Fractured samples from several rock types have been collected and profiled to determine the range of these three parameters in nature. It is shown how model surfaces can be generated on a computer, allowing future detailed study of the mechanical and transport properties of single fractures and the scale dependence of these properties.

Paper number 94JB03262.
0148-0227/95/94JB-03262$05.00

Background

Surface Roughness and Fracture Properties

Mechanical properties. A microscopic model of contact of rough surfaces based on the studies of Hertz [see *Timoshenko and Goodier*, 1970; *Mindlin*, 1949; *Mindlin and Deresiewicz*, 1953] has been shown to successfully describe the elastic properties of a single fracture including both normal and shear stiffness [*Brown and Scholz*, 1985; *Brown and Scholz*, 1986; *Yoshioka and Scholz*, 1989a; *Yoshioka and Scholz*, 1989b]. The surface contact model has a long history in engineering studies of friction and wear and was first presented in its present form by *Greenwood and Williamson* [1966] and first applied to rock fractures by *Walsh and Grosenbaugh* [1979]. Variations of the model have been studied by others [e.g., *Swan*, 1981; *Swan and Zongqi*, 1985]. In the model a fracture is comprised of two contacting rough surfaces, which may or may not be correlated with each other. One major result is that the mechanical properties are largely determined by the sum of the heights of both surfaces, termed the "composite topography." If the heights of the surfaces are $h_1(x, y)$ and $h_2(x, y)$ measured relative to a reference for each surface (such as the mean level) with positive values facing outward from the solid, then the composite topography is defined as $h_C(x, y) = h_1(x, y) + h_2(x, y)$ (Figure 1). The spatial distribution of apertures (when there is no contact) is simply the negative of the composite topography. For this reason, the terms aperture and composite topography are used almost interchangeably. The normal contact of two rough surfaces is equivalent to the contact of the composite topography with a flat surface. The composite topography contains only the mismatched part of the surface roughness. The microscopic model shows that the elastic properties of a fracture are determined largely by the mismatched part of

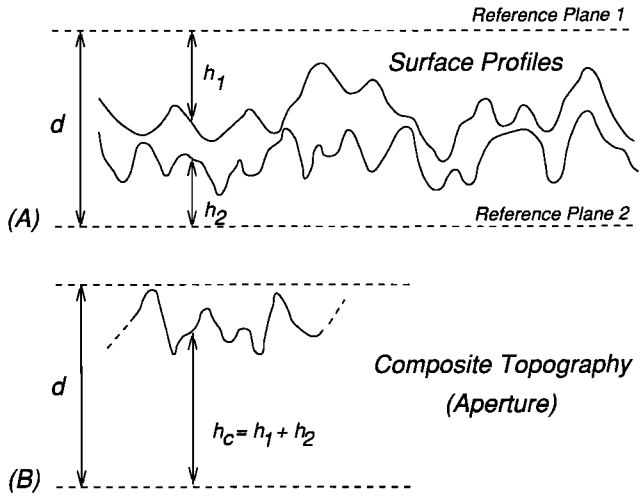

Figure 1. (a) Schematic cross section through a fracture. The surface heights h_1 and h_2 are measured from parallel reference planes fixed in each surface. The separation between these reference planes is d. (b) The "composite topography" h_c of a fracture is defined as the sum of the heights of both surfaces at each position along the fracture plane. The local maxima of the composite topography are the places where the surfaces are closest together (potential contacts). The local aperture of the fracture is obtained by simply subtracting the composite topography h_c from the separation between the reference planes d.

the surface roughness, with the matched wavelengths (where the two surfaces are parallel) having little effect. The surface topography parameters appearing in the model include the number of contacts per unit area, the standard deviation of asperity heights, the probability density function for asperity heights, and the mean radius of curvature of the contacting asperities. The model presented in this paper considers only the spatial statistics of the undeformed aperture distribution and does not predict the mean value of the aperture when two fracture surfaces are pressed together under normal stress. A discussion of surface contact mechanics is beyond the scope of this paper.

Friction is known to depend on the real area of contact of the two surfaces. Thus one might assume that shear strength depends on the same parameters as the elastic properties with an additional significant dependence on the slopes of the individual surfaces, if the surfaces are partly matched and nonplanar. This dependence of shear strength on surface slope is suggested by the analysis of the data of *Barton and Choubey* [1977] by *Tse and Cruden* [1979]. A promising microscopic model for the frictional shear strength has been developed [*Yoshioka and Scholz*, 1989a; *Yoshioka and Scholz*, 1989b].

Transport properties. Fractures often control the fluid flow properties of a rock mass. Knowledge of the hydraulic conductivity of a single fracture is required for meaningful study of fluid flow through fracture systems. Measurement of the electrical conductivity is a possible way to estimate the hydraulic properties both quickly and inexpensively.

In terms of fluid flow and transport, rock fractures are commonly described by the parallel plate model, where the fracture surfaces are smooth and parallel with constant separation or aperture. For this geometry, the steady state solution of the Navier-Stokes equations for laminar flow yields the cubic law, where the volume flow rate is proportional to the cube of the aperture. If the space between the plates is filled with an electrolyte, then we find from Ohm's law that the electric current is proportional to the first power of the aperture.

The parallel plate model can only be considered a qualitative description of flow through real fractures. Real fracture surfaces are not smooth parallel plates but are rough and contact each other at discrete points. Fluid particles and ions are expected to take a tortuous path when moving through a real fracture; thus deviations from the parallel plate model are expected. Taking the spatial variation of the aperture into consideration, laminar flow between rough surfaces has been studied theoretically, numerically, and experimentally [e.g., *Walsh*, 1981; *Brown*, 1987; *Pyrak-Nolte et al.*, 1987; *Pyrak-Nolte et al.*, 1988; *Brown*, 1989; *Stesky*, 1986; *Zimmerman et al.*, 1992; *Olsson and Brown*, 1993]. These studies confirm that surface roughness plays an important role and can lead to a significant departure from the parallel plate model. The spatial variation in aperture combined with the contrast between the cubic dependence of the volume flow rate and the linear dependence of the electric current on the fracture aperture has some important consequences in using electrical geophysical methods in quantifying fluid flow.

These physical models and observations indicate that the measurement of the roughness of fracture surfaces should include the description of both the topography of the individual surfaces and their degree of mismatch.

Roughness Measures in Conventional Tribology

The field of tribology encompasses the study of friction, wear, and elastic and plastic contact between rough surfaces. Surface roughness has been recognized as an important parameter to understand in studying these processes. *Thomas* [1982] gives a complete review of surface roughness measurement in the field of tribology. Surface roughness is most commonly measured by profilometry, where a sharp stylus is dragged over the surface along a straight line to record the surface height in the form of a profile. The deviation of a surface from its mean plane as determined from these profiles is assumed to be a random process for which statistical parameters such as the variances of height, slope, and curvature are used for characterization. The theories describing surface contact mentioned above use these parameters for their analysis. There are myriad surface roughness standards which have evolved from different applications. *Thomas* [1982] describes more than 20 of these standards, which include measures such as the average deviation from the mean (also known as the root-mean-square or rms roughness) and peak-to-valley height.

It has been found for many rough surfaces, especially those formed in part by natural processes such as fractures in rock, that the rms roughness, for example, is a function of the length of the sample [e.g., *Sayles and Thomas*, 1978; *Brown and Scholz*, 1985; *Power and Tullis*, 1991]. Consequently, instruments with different resolutions and scan lengths yield different values for these parameters for the same surface.

The conventional methods of surface roughness characterization are therefore plagued with inconsistencies. The underlying problem with the conventional methods is that although rough surfaces contain roughness components at a large number of length scales, each particular roughness measure depends on only a few particular length scales, which are determined by the resolution and dynamic range of the instrument. These difficulties can be overcome when the general nature of surface roughness is understood.

Mathematical Model

General Description of Roughness

It has been thought for some time that a reasonable statistical description of a two-dimensional (2-D) random process (such as the topography of rough surfaces) is given by the specification of two functions: (1) the probability density function for heights and (2) the autocorrelation function [e.g., *Whitehouse and Archard*, 1970] or an equivalent measure: the power spectrum. The probability density function describes the distribution of the surface heights about the mean value without regard to the horizontal spatial position, and the autocorrelation function or the power spectrum describes the texture or spatial correlation of heights on the surface. The power spectrum is the Fourier transform of the autocorrelation function, thus the two are equivalent descriptions of the same aspect of surface texture [*Bendat and Piersol*, 1971; *Båth*, 1974]. When the surface heights have a Gaussian (normal) distribution, then the 2-D surface texture is described accurately by a combination of the mean and standard deviation of the Gaussian distribution and the form of the autocorrelation function. As seen from this study, natural fractures often have Gaussian heights. However, if the height distribution were more complicated, then a complete description of 2-D structure would require more information [*Ripley*, 1981].

Probability density function. From standard statistics, the probability is defined as the ratio of the number of elements of a set conforming to a particular condition to the total number of elements. Thus the probability ranges between 0 and 1. The description of all possibilities is described by the probability density function, which is defined in the following manner. The probability function $P(z)$ associated with the surface height z, is defined as the fraction of the surface having height $\leq z$, with $P(-\infty) = 0$ and $P(\infty) = 1$ (Figure 2). The probability function $P(z)$ is the integral of the probability density function $p(z)$:

$$P(z) = \int_{-\infty}^{z} p(\xi)d\xi. \tag{1}$$

The probability density function is therefore the derivative of the probability function, i.e.

$$p(z) = \frac{dP(z)}{dz}. \tag{2}$$

The value of $p(z)$ represents the fraction of the surface with height between z and $z + dz$ ($z + \Delta z$ in Figure 2). A well-known example of a probability density function is the Gaussian distribution:

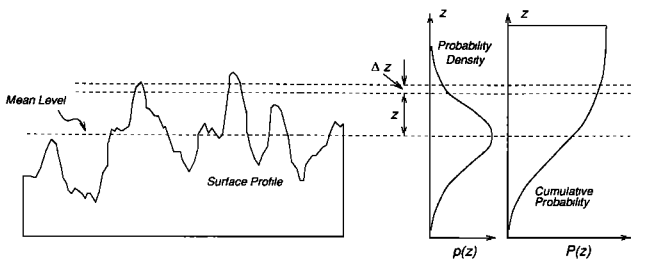

Figure 2. Illustration of the probability functions for surface height. The height of the surface above the mean level is z. The probability density function $p(z)$ is the fraction of the surface in the range z, $z + \Delta z$. The cumulative probability $P(z)$ is the integral of $p(z)$.

$$p(z) = \frac{1}{\sigma\sqrt{2\pi}} e^{-(z-\mu)^2/2\sigma^2}, \tag{3}$$

which is defined completely by the mean μ and the standard deviation σ.

Power spectrum. The power spectrum is the Fourier transform of the autocorrelation function; thus they are equivalent descriptions of the same aspect of surface texture. The power spectrum is more convenient for our purposes. The power spectrum is computed by breaking a time or spatial series, in this case the profile, into a sum of sinusoidal components, each with its own wavelength, amplitude, and phase (Figure 3). The squared amplitude of each component is referred to as its power, and a plot of power versus wavenumber or inverse of wavelength is referred to as the power spectrum. The phase indicates the position of the

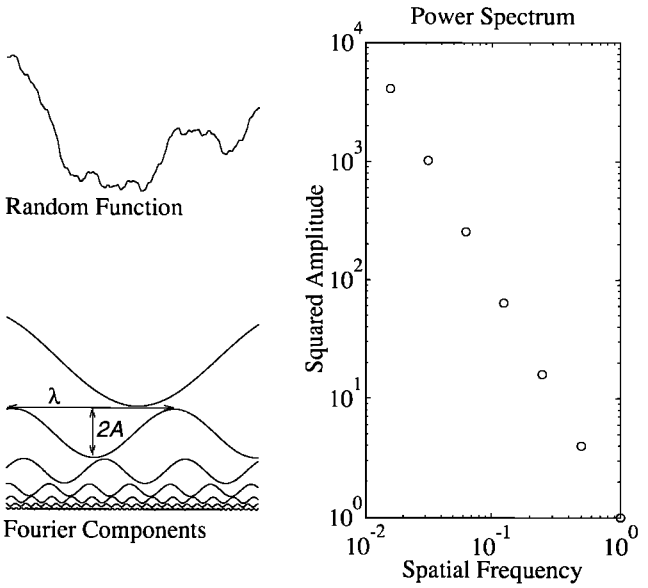

Figure 3. Illustration of the power spectrum of a surface profile. The surface profile (irregular curve, upper left) is decomposed into a series of sinusoidal components (lower left). Each component is characterized by its wavelength (λ), amplitude (A), and phase (relative position of the first peak of the sinusoid to that of all others). A plot of the power A^2 versus the spatial frequency $1/\lambda$ for all sinusoidal components is known as the power spectrum (graph on the right).

first peak of each sinusoid relative to all others. The phase spectrum is a plot of the phase as a function of wavenumber. Phase spectra for rough surfaces are typically random, that is, there is no consistent relation between phase and wavenumber. The power spectrum normalized in a particular way is known as the power spectral density. Excellent introductions to spectral analysis are given by *Bendat and Piersol* [1971] and *Bâth* [1974].

The power spectral density $G(k)$ provides a useful description of the surface roughness if one considers the spectral moments. The moments of the power spectral density function are defined as

$$m_n = \int_{k_0}^{\infty} k^n G(k) dk, \tag{4}$$

where m_n is the nth moment and $k_0 = 2\pi/\lambda_0$ is the wavenumber corresponding to the profile length λ_0. In practice the upper limit of integration is the Nyquist cutoff corresponding to a wavelength of twice the sample interval. By combining the derivative theorem and Parseval's theorem for the Fourier transform [*Bâth*, 1974] we find that m_0 is the variance (mean square value) of heights on the profile, m_2 is the variance of slopes, and m_4 is the variance of curvatures.

In summary, once the probability density function for heights and the autocorrelation function (or the power spectrum) for a surface are known, then a reasonably complete description of the roughness of an individual surface is obtained. To describe an entire fracture (consisting of two juxtaposed surfaces) then one must know the degree of mismatch between the two surfaces. As will be discussed below, the mathematical description of a fracture in rock including this mismatch is quite simple.

Simple Model of Roughness and Scaling for Fractures in Rock

In recent studies, *Brown and Scholz* [1985], *Power et al.* [1987], *Power and Tullis* [1991], and *Power and Tullis* [1992] computed power spectral densities of various natural rock surfaces. The surfaces studied included natural joints in crystalline and sedimentary rock, a bedding plane surface, and frictional wear surfaces. Their results show that there is remarkable similarity among these surfaces. Profiles of these widely different fracture surfaces have decreasing power law power spectra of the form

$$G(k) = Ck^{-\alpha}, \tag{5}$$

where k is the wavenumber related to the wavelength λ according to $k = 2\pi/\lambda$. The exponent α has a fairly limited range (typically between 2 and 3). The power spectrum (and therefore the roughness) can thus be described to first approximation by two parameters: (1) the exponent in the power law α (i.e., the slope of the power spectrum on a log-log plot) and (2) the proportionality constant C (i.e., the intercept of the power spectrum line on a log-log plot).

This power law form of the power spectrum indicates that fracture surface topography can be represented in terms of fractal geometry where the fractal dimension of the surface D is related to the power spectrum exponent as $D = (7-\alpha)/2$ (see discussions by *Mandelbrot* [1983], *Brown and Scholz* [1985], *Brown* [1987], *Brown* [1988], and *Power and Tullis* [1991]). The fractal dimension describes the proportion of high-frequency to low-frequency roughness and is a measure of surface texture. For natural fracture surfaces, D tends to fall approximately in the range $2 \leq D \leq 2.5$, with small values representing smoother surfaces.

Brown et al. [1986] measured matched profiles from both halves of natural joint surfaces, allowing the power spectrum of the aperture or composite topography to be computed as well. This work shows that the aperture distribution has a power law spectrum as well at high spatial frequencies (short wavelengths), but it flattens out at low spatial frequencies (long wavelengths). The crossover between the power law behavior and the flat spectrum allows a mismatch length scale to be defined as the point where the ratio of the aperture spectrum to the spectrum of the individual surfaces reaches 1/2 of its high-frequency value. In the simple model of a rough-walled fracture described in this paper, this length scale is the third and final parameter needed to define the roughness of a fracture. This mismatch length scale is essentially the largest wavelength present in the composite topography with any significant amplitude, and it defines the dominant roughness component affecting the fracture properties.

In summary, to describe a rough-walled fracture in rock, there are three independent parameters to be determined: (1) the exponent in the power law power spectrum, (2) the proportionality constant for the power spectrum, and (3) the mismatch length scale. As will be described later, these three parameters are sufficient to generate realistic computer images of rough fractures using techniques of fractal geometry.

The scale dependence of roughness for this model can be seen by considering the zeroth moment of the power spectrum m_0 as a function of the lower limit of integration k_0 (equation (4)). The profile length λ_0 is related to the lower limit of integration as $\lambda_0 = 2\pi/k_0$. The zeroth moment m_0 is defined as $m_0 = \sigma^2$, where σ^2 is the variance of heights and σ is the standard deviation of heights (also known as the root-mean-square or rms roughness). When the power spectrum is $G(k) = Ck^{-\alpha}$ (i.e., a power law), then for $\alpha > 1$ equation (4) becomes $\sigma \sim \lambda_0^{(\alpha-1)/2}$. This is the scaling law for rms roughness σ for an individual surface. Notice that the two roughness parameters (the proportionality constant C and the exponent α) completely determine the scaling law for the roughness of the individual surfaces. However, we notice that for the aperture of a matched fracture, the power law holds only for wavelengths $\lambda < \lambda_C$, where λ_C is the mismatch length scale. At larger wavelengths, the power spectrum is almost constant. Consideration of equation (4) for this type of spectrum shows that the rms roughness of the aperture scales in a similar manner to the individual surfaces for $\lambda < \lambda_C$ but rapidly approaches an asymptote and is effectively scale independent for larger wavelengths (Figure 4). Thus to the extent that a mechanical property depends only on the rms roughness σ there will be an upper limit to the scale or size effect. However, for a matched fracture undergoing shear displacements the mismatch length scale λ_C increases roughly in proportion to the shear offset, resulting in a coupling of the scale effect to the amount of deformation expected. Regardless, the surface profile data will provide a means to quantitatively model these effects.

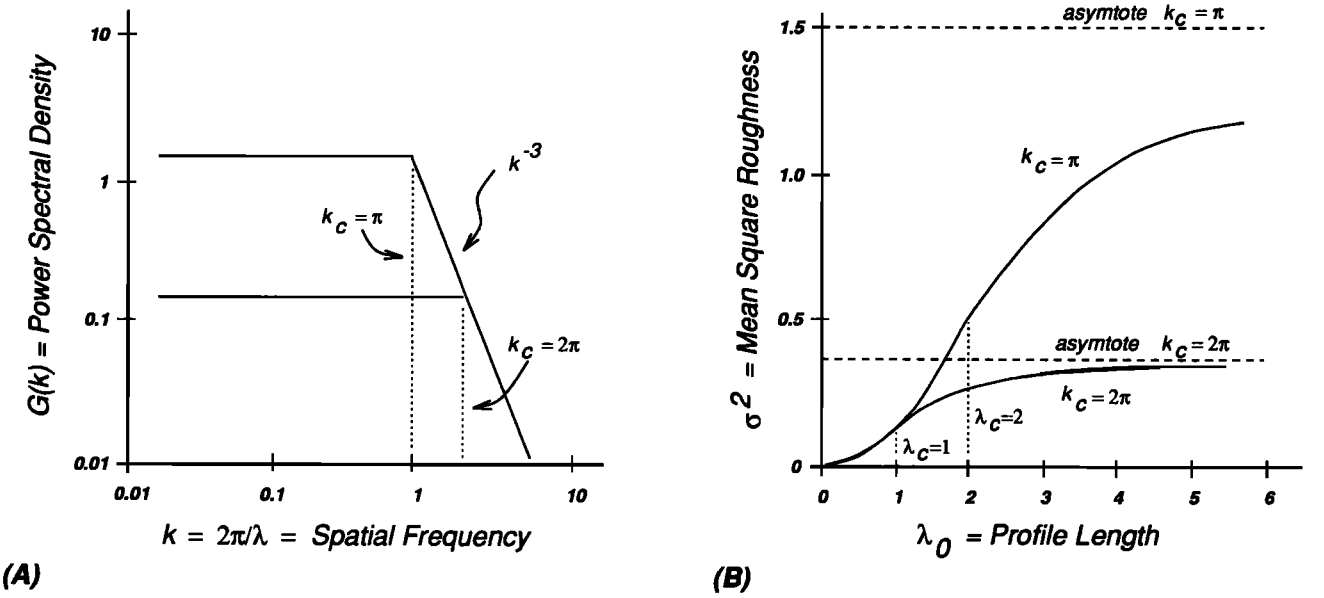

Figure 4. (a) Two hypothetical spectra of the composite topography of two fractures. The power law exponent is -3 for both fractures, but the mismatch length scale $\lambda_c = 2\pi/k_c$ differs by a factor of 2. (b) The scaling laws for surface roughness corresponding to the spectra in Figure 4a. The mean square roughness σ^2 as a function of profile length λ_0 was computed from equation (4). Note that the surface roughness quickly approaches an asymptote for length scales larger than λ_c. This implies that the roughness of the composite topography is not strongly scale dependent at longer wavelengths.

These considerations of scaling point out that two additional parameters are involved in the description of a fracture: the upper and lower limits of integration in (4). These parameters are not characteristics of the surface itself but are nevertheless important in practice. The upper limit of integration depends on the instrument sampling interval or perhaps on some criterion determined by the physics of a problem being studied (*Thomas* [1982] uses the term "functional filtering" to describe the latter), and the lower limit of integration is determined by the specimen size (again determined by the application). Calculation of the spectral moments from (4) requires careful consideration of these integration limits [*Thomas*, 1982]. The power law form of a fracture surface implies that m_0 is highly sensitive to the lower limit of integration (specimen size) and insensitive to the upper limit of integration (sample interval). The higher moments (m_2, m_4, ...) are highly sensitive to the sample interval and insensitive to the specimen size. The spectrum of the composite topography rolls off at low spatial frequencies, making m_0 insensitive to specimen size at length scales larger than the mismatch length.

Aperture Roughness as a Function of Shear Offset

For all applications it is of considerable interest to know the statistical properties of the aperture. For the case of two identical isotropic fractal surfaces slid past one another in shear, a mathematical relation between aperture and offset can be found. *Wang et al.* [1988] considered the relationship between the power spectrum of the aperture $G_f(k)$ to that of the surfaces $G(k)$ as a function of shear offset r. For the aperture resulting from contact of one-dimensional (1-D) linear profiles offset in shear we have

$$G_f(k) = 2\left[1 - \cos(kr)\right] G(k). \tag{6}$$

For the aperture resulting from contact of isotropic 2-D surfaces offset in shear averaged over all profile orientations we have

$$G_f(k) = 2\left[1 - J_0(kr)\right] G(k), \tag{7}$$

where J_0 is the Bessel function of order 0. For a fractal profile or surface, the power spectral density is given by (5) and the spectral moments are given by (4). To find the variance of the aperture m_0, we substitute (5), (6), and (7) into (4) to find

$$m_0 = 2C \int_{k_0}^{\infty} \left[1 - \cos(kr)\right] k^{-\alpha} dk \tag{8}$$

and

$$m_0 = 2C \int_{k_0}^{\infty} \left[1 - J_0(kr)\right] k^{-\alpha} dk. \tag{9}$$

These expressions can be integrated to yield the dependence of aperture on shear offset. If the offset r is sufficiently small compared to the sample length $2\pi/k_0$, then reasonable approximations can be obtained by assuming $k_0 = 0$. In this case we find

$$m_0 = -C \frac{\pi r^{\alpha-1} \sec(\alpha\pi/2)}{\Gamma(\alpha)} \tag{10}$$

for profiles and

$$m_0 = -C \frac{\pi r^{\alpha-1} \sec(\alpha\pi/2)}{2^{\alpha-1}\left[\Gamma\left(\frac{\alpha+1}{2}\right)\right]^2} \tag{11}$$

for the average over 2-D aperture. In these expressions Γ is the standard gamma function.

Computer Simulation of a Fracture With Anisotropic Roughness

As described above, measurements and analysis of surface profiles of natural fractures have established that fracture surface topography can be represented in terms of fractal geometry. Linear profiles exhibit decaying power law power spectral density functions of the same form as fractal surfaces (equation (5)). Additionally, the two surfaces composing a fracture are often closely matched at long wavelengths and mismatched at small wavelengths, resulting in an aperture distribution whose spectrum has the form (5) at small wavelengths but flattens out at long wavelengths.

One method of computing the power spectral density function just discussed is to take the Fourier transform of the topography [e.g., *Bendat and Piersol*, 1971]. This calculation is the generalization of Fourier analysis and results in a series of sinusoidal components, which can be characterized by their wavelength, amplitude, and relative phase. This information, collectively known as the amplitude spectrum, is a series of complex numbers which contains both amplitude and phase information. The power spectrum is the modulus or square of the various amplitude components. Using this fact, *Peitgen and Saupe* [1988] present a spectral synthesis method to generate computer models of isotropic fractal surfaces. The method works by constructing a two-dimensional complex amplitude spectrum with a random phase component which obeys (5). The fractal surface is just the inverse Fourier transform of the amplitude spectrum. The standard deviation of the surface height is set after the inverse transform is taken.

We may also wish to consider the possible effect of anisotropic roughness on the physical properties of fractures. Therefore the spectral synthesis method is used but with (5) modified to include anisotropy as follows:

$$G(k) \propto \left[(k_x/a)^2 + (k_y/b)^2\right]^{-(3.5-D)}. \qquad (12)$$

The ratio b/a is the degree of anisotropy. For $b/a < 1$ the anisotropy is transverse to x, for $b/a = 1$ the surface is isotropic, and for $b/a > 1$ the anisotropy is parallel to x. In this model the surface has the same fractal dimension in all directions (i.e., the same proportional change in amplitude with a corresponding change in frequency), but the absolute amplitude of the sinusoidal components differs by a constant factor in each direction.

To force two surfaces of a fracture to be matched at long wavelengths, the two surfaces are generated with the same random number seed and anisotropy factor, but the random phase spectrum is identical only above a particular wavelength. The length scale at which the phase spectrum of the two surfaces becomes different is defined as the mismatch length scale. With this modification in the phase spectrum, the power spectrum of the resulting fracture aperture closely resembles that observed for natural fractures by *Brown et al.* [1986].

A computer algorithm implementing this model is presented in Figure 5. To produce two surfaces of a mated fracture, the program would be run twice: first without modification of the phase spectrum random number sequence and then again with the random number sequence modified at a specified mismatch length scale. An example of a pair of fracture surfaces and the resulting aperture distribution generated in this manner is shown in Figure 6.

Range of Model Parameters in Nature

Samples

Samples from 23 natural rock joints have been collected for a study of the roughness and degree of mismatch of fracture surfaces. Most of the samples were obtained from roadside outcrops in central New Mexico near Albuquerque. The samples were taken from members of systematic joint sets and are thus considered naturally occurring. A few samples were taken from drill core. The samples mostly consisted of 2.54 cm (1 inch) diameter cores taken so that the fracture planes were approximately along the diameter and parallel to the axis of the cores. Descriptions of the samples are given in Table 1.

Profilometer

The topography of each fracture surface was measured with a noncontacting laser profilometer. This instrument consists of a precision three-axis positioning system which moves a laser distance measurement probe over the surface, recording surface height. The probe is moved along parallel straight lines to record a series of one-dimensional surface profiles. The principle of operation of the laser sensor of this instrument is described in detail by *Huang et al.* [1988].

The profilometer can sample a 15 × 15 cm area on a minimum grid spacing of 25 μm. The spot size of the laser is 25 μm, which fixes the spatial resolution in the fracture plane at this same value. The maximum peak to valley height range is 10 cm. The theoretical height resolution is 3.8 μm, but the rms noise level due to mechanical vibration is 5 μm with a maximum peak to valley value of 20 μm (this peak to valley value is the maximum uncertainty of the height measurement).

The samples were mounted in the profilometer in such a way as to allow matched pairs of profiles from each surface to be closely refitted in the subsequent analysis. Topographic heights were sampled every 25 μm along each profile. Several preliminary data processing steps were done once the profiles were taken. First, each pair of profiles from the two halves of the fracture were fitted together and the standard deviation of the aperture distribution (local distance between the surfaces) was computed. Then the two profiles were repeatedly shifted relative to one another and the aperture distribution was computed until the best match was obtained as indicated by the minimum standard deviation of the aperture. The two resulting matched profiles were then truncated to the same length and the mean level and the linear slope were removed from both profiles and the aperture distribution. Table 2 indicates the total number of matched pairs of profiles taken from each sample (N) and the final truncated length of these profiles used in the analysis (L).

```
ALGORITHM  FractureSurface(X,N,H,Seed,Aniso,Mismatch)
Arguments  X[][]          array of complex numbers of size N×N
           N              size of array X along one dimension
           H              0<H<1 determines fractal dimension D=3-H
           Seed           random number seed
           Aniso          anisotropy factor
           Mismatch       wavenumber determining mismatch of 2 surfaces
Globals    MaxSeed        maximum random number seed value
Variables  i,j,i0,j0      integers
           temp           real
           Rad, Phase     polar coordinates of Fourier coefficient
           A[][]          array of complex numbers of size N×N
Functions  InverseFFT2D()  inverse 2-D fast Fourier transform
           RandNum1(),     two independent random number generators
           RandNum2()        returning real numbers in range 0-1
BEGIN
  InitRandNum1(Seed);
  InitRandNum2(MaxSeed * RandNum1());
  FOR i:=0 TO N/2 DO
    FOR j:=0 TO N/2 DO
      IF (sqrt(i*i+j*j) < Mismatch) THEN
        Phase := 2 * 3.14159 * RandNum1();
      ELSE
        Temp := RandNum1();
        Phase := 2 * 3.14159 * RandNum2();
      END IF
      IF (i=0 OR j=0) THEN
        Rad := 0;
      ELSE
        Rad := power( i*i + j*j/(Aniso*Aniso), -(H+1)/2 );
      END IF
      A[i][j] := ( Rad*cos(Phase), Rad*sin(Phase) );
      IF (i=0) THEN
        i0 := 0;
      ELSE
        i0 := N-i;
      END IF
      IF (j=0) THEN
        j0 := 0;
      ELSE
        j0 := N-j;
      END IF
      A[i0][j0] := ( Rad*cos(Phase), -Rad*sin(Phase) );
    END FOR
  END FOR
  A[N/2][0].imag := 0;
  A[0][N/2].imag := 0;
  A[N/2][N/2].imag := 0;
  FOR i:=1 TO N/2-1 DO
    FOR j:=1 TO N/2-1 DO
      IF(sqrt(i*i+j*j) < Mismatch) THEN
        Phase := 2 * 3.14159 * RandNum1();
      ELSE
        Temp := RandNum1();
        Phase := 2 * 3.14159 * RandNum2();
      END IF
      Rad := power( i*i + j*j/(Aniso*Aniso), -(H+1)/2 );
      A[i][N-j] := ( Rad*cos(Phase), Rad*sin(Phase) );
      A[N-i][j] := ( Rad*cos(Phase), -Rad*sin(Phase) );
    END FOR
  END FOR
  InverseFFT2D(A,X,N);
END
```

Figure 5. Pseudocode for generating rough, anisotropic, and mismatched fracture surfaces.

A typical example of the best fit of two profiles from one of these fractures (MVA1) and the resulting composite topography is shown in Figure 7.

Analysis

Once the matched profiles and the composite topography were obtained for each surface, several surface roughness

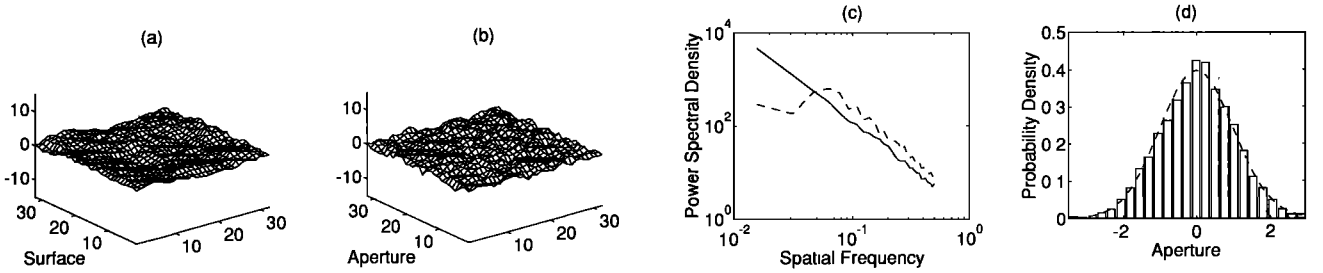

Figure 6. (a) Fracture surface. (b) Resulting aperture distribution formed by contact of two surfaces mismatched at a length scale of 1/4 of the surface size. Note that the dominant wavelength of features in the aperture distribution is approximately 1/4 of the fracture size. (c) Power spectral density function of surface (Figure 6a) (solid line) and aperture distribution (Figure 6b) (dashed line). The curves begin to cross over at a frequency corresponding to approximately 1/4 of the surface size. (d) Probability density function for the aperture distribution (bars) compared to a Gaussian distribution (dashed line). Since this figure is the product of numerical simulation, the length units are arbitrary.

Table 1. Fracture Samples

Sample	Description
BT1	natural joint in welded member of Bandelier Tuff, Los Alamos, NM; fracture perpendicular to bedding
BT2	natural joint in welded member of Bandelier Tuff, Los Alamos, NM; fracture perpendicular to bedding
EE2	natural joint in granodiorite from Hot Dry Rock Borehole EE-2 (4420.8 m) near Los Alamos, NM [*Brown et al.*, 1986]; slightly mineralized with chlorite and epidote
EE3A	natural joint in granodiorite from Hot Dry Rock Borehole EE-3A (2880.4 m) near Los Alamos, NM [*Brown et al.*, 1986]; slightly mineralized with chlorite and epidote
G4300	natural joint in welded tuff from borehole USW G-4 (91.7 m) at Yucca Mountain, NV [*Spengler and Chornak*, 1984]
G41069	natural joint in welded tuff from borehole USW G-4 (325.9 m) at Yucca Mountain, NV [*Spengler and Chornak*, 1984]
G41615	natural joint in welded tuff from borehole USW G-4 (492.4 m) at Yucca Mountain, NV [*Spengler and Chornak*, 1984]
LAB1	natural hexagonal cooling joint from a surface basalt flow near Los Alamos, NM
LAB2	natural hexagonal cooling joint from a surface basalt flow near Los Alamos, NM
LB1	natural fracture in sandstone from La Bajada Hill between Albuquerque and Santa Fe, NM; fracture intersects a discrete fault plane at a high angle; sample taken adjacent to fault
LIC	natural joint in metasediment (volcanic graywacke ?) from Lake Irwin, CO
MVA1	natural joint in a rhyolitic dike near Madrid, NM
MVA2	natural joint in a rhyolitic dike near Madrid, NM
MVA3	natural joint in a rhyolitic dike near Madrid, NM
MVB1	natural joint in a rhyolitic dike near Madrid, NM; In situ shear offset on joint of 2-3 mm; matched profiles measured in this offset condition, perpendicular to offset
MVB2	natural joint in a rhyolitic dike near Madrid, NM
ORYX	natural joint from drill core in Austin Chalk [*Olsson and Brown*, 1993]; nonmineralized
SM1	natural joint in rhyolitic tuff from the San Mateo Mountains, NM; fracture perpendicular to bedding; strongly anisotropic surface texture with linear steps in topography at intersections with bedding planes; profiles perpendicular to steps
SM2	same sample as SM1 above, but profiles parallel to steps in topography
SSS1	natural joint in siltstone from Sandia Mountains near Cedar Crest, NM
UCB720	induced fracture in Westerly Granite [*Chen*, 1992; *Chen and Spetzler*, 1993]; fracture formed at $\sim$ 30° to the principal stress under polyaxial loading; no shear offset after fracture formation; profiles parallel to impending slip direction
UCB725	induced fracture in Westerly Granite [*Chen*, 1992; *Chen and Spetzler*, 1993]; fracture formed at $\sim$ 30° to the principal stress under polyaxial loading; after formation fracture was allowed to slide $\sim$ 100 μm under shear load; all slip was accomodated by one stick-slip event; profiles parallel to slip direction
UCB96	induced fracture in Westerly Granite [*Chen*, 1992; *Chen and Spetzler*, 1993]; fracture formed at $\sim$ 18° to the principal stress under triaxial loading; after formation fracture was allowed to slide $\sim$ 800 μm under shear load; all slip was accomodated by stable sliding; profiles parallel to slip direction

parameters were derived (Table 2). These include the standard deviation of the profile at length L, σ_p; the standard deviation of the composite topography at length L, σ_a; two estimates of the fractal dimension, D_{lin} and D_{log}, and two estimates of the mismatch length scale, λ_c^1 and λ_c^2. In the following sections, the definitions of these parameters are given.

Standard deviations. For each surface, all profiles (top and bottom) were considered together in the calculation of the sample standard deviation of surface heights using the standard statistical definition as the average deviation from the mean. Similarly, all profiles of composite topography were considered together. Note that knowing the standard deviation of the surface profiles at a given profile length is equivalent to knowing the constant C in (5). The probability density functions for the composite topography are nearly symmetrical and in most cases can be approximated by a Gaussian distribution. The relatively poor degree of symmetry seen in Figure 7 is not typical of the other fractures studied.

Fractal dimension. For each surface profile, the power spectral density was computed using the same method as that of *Brown and Scholz* [1985]. This consists of removing the mean and linear trend from the profiles, windowing the result with a 10% cosine tapered window, applying the Fourier transform, squaring the result to obtain power, cor-

Table 2. Fracture Surface Roughness Parameters

Sample	N	L, mm	σ_p, mm	σ_a, mm	D_{lin}	D_{log}	λ_c^1, mm	λ_c^2, mm
BT1	10	13.0	0.0978	0.041	1.47 ± 0.184	1.41 ± 0.331	1.19	0.183
BT2	10	13.0	0.0682	0.0514	1.53 ± 0.174	1.45 ± 0.312	2.67	0.506
EE2	10	13.0	0.222	0.0587	1.24 ± 0.223	1.09 ± 0.401	0.529	0.180
EE3A	10	13.0	0.111	0.0487	1.37 ± 0.201	1.32 ± 0.362	0.805	0.131
G4300	5	52.0	0.758	0.375	1.35 ± 0.102	1.30 ± 0.252	7.42	3.3
G41069	5	52.0	0.702	0.190	1.26 ± 0.11	1.17 ± 0.271	3.73	0.97
G41615	5	52.0	0.962	0.02	1.33 ± 0.104	1.27 ± 0.257	2.74	0.748
LAB1	10	13.0	0.233	0.0784	1.17 ± 0.234	1.15 ± 0.421	1.02	0.291
LAB2	10	13.0	0.141	0.054	1.28 ± 0.216	1.23 ± 0.389	0.643	0.222
LB1	10	13.0	0.156	0.136	1.49 ± 0.178	1.52 ± 0.32	4.12	0.894
LIC	10	13.0	0.085	0.0432	1.43 ± 0.19	1.36 ± 0.341	1.63	0.653
MVA1	10	13.0	0.0985	0.0315	1.35 ± 0.205	1.34 ± 0.368	0.624	0.274
MVA2	10	13.0	0.204	0.059	1.36 ± 0.202	1.40 ± 0.363	0.993	0.266
MVA3	10	13.0	0.0864	0.0218	1.37 ± 0.199	1.36 ± 0.359	0.41	0.18
MVB1	10	13.0	0.0668	0.0813	1.37 ± 0.201	1.34 ± 0.361	‡	1.81
MVB2	10	13.0	0.0894	0.033	1.44 ± 0.187	1.35 ± 0.337	1.09	0.381
ORYX	10	26.0	0.104	0.0173	1.64 ± 0.11	1.41 ± 0.23	0.386	0.175
SM1	10	26.0	0.189	0.134	1.30 ± 0.152	1.25 ± 0.316	0.761	0.293
SM2	10	26.0	0.147	0.0501	1.45 ± 0.136	1.23 ± 0.282	2.39	0.466
SSS1	10	13.0	0.0454	0.0463	1.49 ± 0.179	1.48 ± 0.321	2.67	0.769
UCB720	3	13.0	0.201	0.162	1.60 ± 0.166	1.51 ± 0.297	5.99	1.3
UCB725	3	13.0	0.188	0.138	1.57 ± 0.171	1.49 ± 0.306	3.51	0.693
UCB96	3	13.0	0.204	0.183	1.35 ± 0.211	1.21 ± 0.378	‡	0.714

N is the number of profiles; L is the profile length; σ_p is the average standard deviation of the N profiles at length L; σ_a is the standard deviation of the composite topography at length L; D_{lin} and D_{log} are two estimates of the fractal dimension; and λ_c^1 and λ_c^2 are two estimates of the mismatch length scale. Mismatch lengths indicated by the symbol ‡ are greater than or equal to the profile length L. See text for further discussion.

recting for the taper, and normalizing to get spectral density. All spectra from a given surface were then averaged, frequency by frequency, to produce a smoothed estimate for the surface. The result is approximately a power law (e.g., Figure 8). Two straight lines were fit to these functions in log-log space, and the fractal dimension of the profile was calculated from the slope (α) of these lines from the relation $D = (5 - \alpha)/2$ (note that this relation for a profile is different from that quoted earlier for the fractal dimension of a surface). The difference between the two linear fits is in the weighting function used. The estimate D_{lin} used a uniform weight for all frequencies, the estimate D_{log} weighted the fit by the logarithm of the frequency. The reason for the log weighting is as follows. The frequency values resulting from the Fourier transform are equally spaced; thus there are many more data points at the high-frequency end of a log-log plot. This high-frequency (small wavelength) data is susceptible to contamination by mechanical and electrical instrument

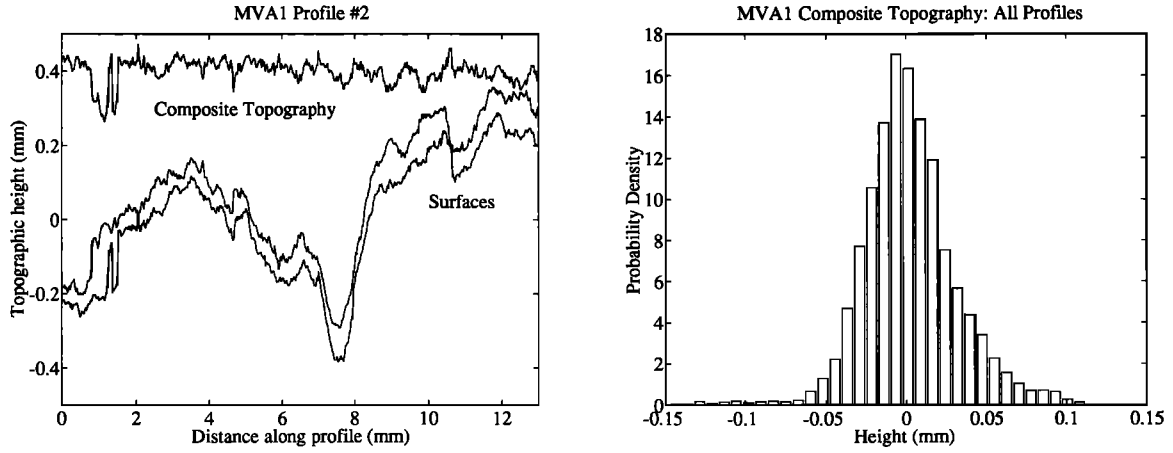

Figure 7. (left) Pair of matched profiles and resulting composite topography distribution for fracture MVA1. (right) Probability density function for the composite topography.

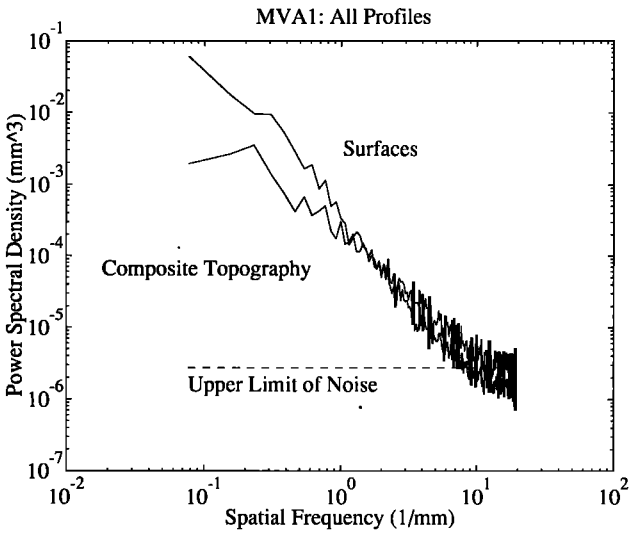

Figure 8. Power spectral densities for fracture MVA1. Note the concave upward character at high frequencies, indicating some possible contamination by noise. The upper limit of the observed "white" instrument noise spectrum (from electrical and mechanical sources) is shown in the horizontal dashed line and is found to intersect the roughness spectra at a wavelength near 100 μm.

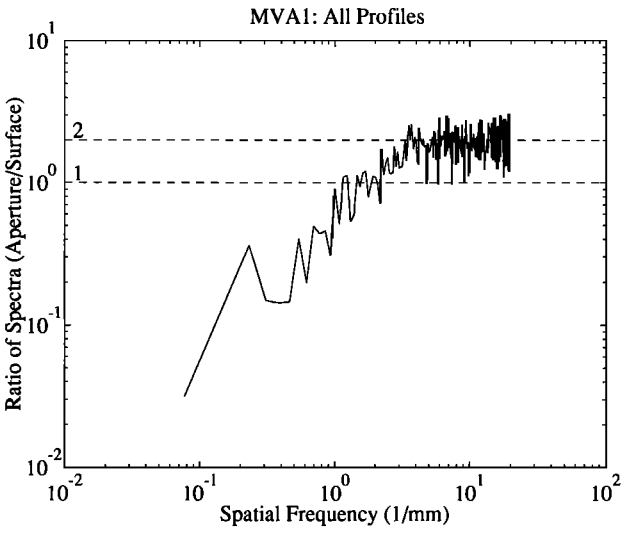

Figure 9. Ratio of spectra for fracture MVA1. The ratios 1.0 and 2.0 used to estimate the mismatch length scale are indicated by dashed lines.

noise making the log-log plot nonlinear (concave upward) at the high-frequency end (Figure 8). Simply fitting a straight line to data with uniform weights gives more emphasis to the possibly noisy high-frequency range. By making the lower frequencies more important as in the logarithmic weighting, this problem is reduced. In Table 2, where the two estimates are close to the same, then the power spectrum is extremely linear, if they are different, then D_{log} better represents the low spatial frequency (long wavelength) behavior. The noise spectrum is "white," i.e., has no dependence on frequency. As seen in Figure 8, the surfaces and composite topography have comparable amplitude to the noise only at the highest frequencies. Thus the low-amplitude noise present in the data does not significantly affect any surface roughness features with wavelengths larger than 100 μm. The presence of low level noise does not change any conclusions about the applicability of the model.

Mismatch length scale. A smoothed estimate of the power spectral density of the composite topography was calculated in an identical manner as for the surface profiles. The ratio of the composite topography spectrum to the surface spectrum was then calculated (e.g., Figure 9). At high frequencies this ratio approaches the value of 2; and at low frequencies it falls off to values much less than 1. In Table 2, the parameter λ_c^1 is the wavelength at which the ratio reaches the value 1, and the parameter λ_c^2 is the wavelength at which the ratio departs significantly from the value 2.0. These choices were made by eye.

Discussion

Because many different fractures from several origins were studied, these results represent the typical values of the roughness parameters for rock joints encountered in nature. Several features deserve to be emphasized. First, all fracture surfaces encountered can be described, to a first approximation, by a self-affine fractal model, i.e., they have a power law power spectrum [e.g., *Brown*, 1987]. Second, the probability density functions of the composite topography are approximately symmetric, reminiscent of the Gaussian bell-shaped curve. No strong evidence for lognormal apertures was seen. Finally, the surfaces of most rock joints are well matched with one another above a scale of a few millimeters. Notable exceptions to this conclusion are those surfaces obviously misaligned in outcrop (e.g., MVB1) and surfaces known to have undergone considerable frictional wear (LB1 and UCB96). One fracture in tuff (G4300) had a large mismatch as well, in part due to the highly heterogeneous lithology and void geometry. The close adherence of the surfaces and composite topography to the mathematical model combined with the typical small mismatch length scale suggests that, unlike the fractal surfaces, the aperture distribution is statistically stationary (not scale dependent) for sample sizes greater than a few centimeters. Longer profiles would have to be studied to confirm the generality of this result.

Summary

A simple mathematical model of a rough fracture was described which requires the specification of only three main parameters. Profiles of many natural fractures were analyzed to determine the range of these parameters in nature. To a first approximation, the fracture surface data fit the model reasonably well. It was shown that this model can be implemented on a computer allowing future detailed study of the mechanical and transport properties of single fractures and the scale dependence of these properties.

Acknowledgements. I wish to thank Bob Hardy for his able technical support in the lab and field. This work was

performed at Sandia National Laboratories supported by the U.S. Department of Energy under contract DE-AC04-94AL85000. Parts of this work were supported by the DOE Office of Basic Energy Sciences Geosciences Research Program, and parts were supported by the Yucca Mountain Site Characterization Project WBS 1.2.3.2.7.1.4. The data contained in this report are not qualified and are not to be used for licensing.

References

Barton, N., and V. Choubey, Shear strength of rock joints in theory and practice, *Rock Mechanics*, *10*, 1-54, 1977.

Båth, M., *Spectral Analysis in Geophysics*, 563 pp., Elsevier, New York, 1974.

Bendat, J. S., and A. G. Piersol, *Random Data, Analysis and Measurement Procedures*, 407 pp., John Wiley and Sons, New York, 1971.

Brace, W. F., Permeability of crystalline and argillaceous rocks, *Int. J. Rock Mech. Min. Sci. Geomech. Abstr.*, *17*, 241-251, 1980.

Brown, S. R., A note on the description of surface roughness using fractal dimension, *Geophys. Res. Lett.*, *14*, 1095-1098, 1987.

Brown, S. R., Correction to "A note on the description of surface roughness using fractal dimension", *Geophys. Res. Lett.*, *15*, 286, 1988.

Brown, S. R., Transport of fluid and electric current through a single fracture, *J. Geophys. Res.*, *94*, 9429-9438, 1989.

Brown, S. R., and C. H. Scholz, Broad bandwidth study of the topography of natural rock surfaces, *J. Geophys. Res.*, *90*, 12,575-12,582, 1985.

Brown, S. R., and C. H. Scholz, Closure of rock joints, *J. Geophys. Res.*, *91*, 4939-4948, 1986.

Brown, S. R., R. L. Kranz, and B. P. Bonner, Correlation between the surfaces of natural rock joints, *Geophys. Res. Lett.*, *13*, 1430-1433, 1986.

Chen, G., Deformation of Fractured Westerly Granite under Low Confining Stress Conditions, Ph.D. thesis, Univ. of Colo., Boulder, 1992.

Chen, G., and H. A. Spetzler, Topographic characteristics of laboratory-induced shear fractures, *Pure Appl. Geophys.*, *140*, 123-135, 1993.

Goodman, R. E., *Methods of Geological Engineering in Discontinuous Rocks*, 472 pp., West Publishing, New York, 1976.

Greenwood, J. A., and J. Williamson, Contact of nominally flat surfaces, *Proc. R. Soc. London, A*, *295*, 300-319, 1966.

Huang, C., I. White, E.G. Thwaite, and A. Bendeli, A non-contact laser system for measuring soil surface topography. *J. Soil Sci. Soc. Am.*, *52*, 350-355, 1988.

Kranz, R. L., A. D. Frankel, T. Engelder, and C. H. Scholz, The permeability of whole and jointed Barre granite, *Int. J. Rock Mech. Min. Sci. Geomech. Abstr.*, *16*, 225-234, 1979.

Mandelbrot, B. B., *The Fractal Geometry of Nature*, 468 pp., W. H. Freeman, New York, 1983.

Mindlin, R. D., Compliance of elastic bodies in contact, *J. Appl. Mech.*, *16*, 259-269, 1949.

Mindlin, R. D. and H. Deresiewicz, Elastic spheres in contact under varying oblique forces, *J. Appl. Mech.*, *20*, 327-344, 1953.

Olsson, W. A., and S. R. Brown, Hydromechanical response of a fracture undergoing compression and shear, *Int. J. Rock Mech. Min. Sci. Geomech. Abstr.*, *30*, 845-851, 1993.

Peitgen, H.-O., and D. Saupe, *The Science of Fractal Images*, pp. 71-136, Springer-Verlag, New York, 1988.

Power, W. L., and T. E. Tullis, Euclidian and fractal models for the description of rock surface roughness, *J. Geophys. Res.*, *96*, 415-424, 1991.

Power, W. L., and T. E. Tullis, The contact between opposing fault surfaces at Dixie Valley, Nevada, and implications for fault mechanics, *J. Geophys. Res.*, *97*, 14425-15435, 1992.

Power, W. L., T. E. Tullis, S. R. Brown, G. N. Boitnott, and C. H. Scholz, Roughness of natural fault surfaces, *Geophys. Res. Lett.*, *14*, 29-32, 1987.

Pyrak-Nolte, L. J., Myer, L. R., Cook, N. G. W., and P. A. Witherspoon, Hydraulic and mechanical properties of natural fractures in low permeability rock, in *Proceedings of the Sixth International Congress on Rock Mechanics*, edited by G. Herget and S. Vongpaisal, pp. 225-231, A. A. Balkema, Rotterdam, Netherlands, 1987.

Pyrak-Nolte, L. J., N. G. W. Cook, and D. D. Nolte, Fluid percolation through single fractures, *Geophys. Res. Lett.*, *15*, 1247-1250, 1988.

Ripley, B. D., *Spatial Statistics*, p. 10, John Wiley, New York, 1981.

Sayles, R. S., and T. R. Thomas, Surface topography as a non-stationary random process, *Nature*, *271*, 431-434, 1978.

Spengler, R. W., and M. P. Chornak, Stratigraphic and structural characteristics of volcanic rocks in core hole USW G-4, Yucca Mountain, Nye County, Nevada, with a section on geophysical logs by D. C. Muller and J. Kibler, *U.S. Geol. Surv. Open File Rep., 84-789*, 1984.

Stesky, R. M., Electrical conductivity of brine-saturated fractured rock, *Geophysics*, *51*, 1585-1593, 1986.

Swan, G., Tribology and the characterization of rock joints, *Proc. U.S. Rock Mech. Symp., 22nd*, 402-407, 1981.

Swan, G., and S. Zongqi, Prediction of shear behavior of joints using profiles, *Rock Mech. Rock Eng.*, *18*, 183-212, 1985.

Thomas, T. R., *Rough Surfaces*, 261 pp., Longman, New York, 1982.

Timoshenko, S. P., and J. N. Goodier, *Theory of Elasticity*, 567 pp., McGraw-Hill, New York, 1970.

Tse, R., and D. M. Cruden, Estimating joint roughness coefficients, *Int. J. Rock Mech. Min. Sci. Geomech. Abstr.*, *16*, 303-307, 1979.

Walsh, J. B., Effect of pore pressure and confining pressure on fracture permeability, *Int. J. Rock Mech. Min. Sci. Geomech. Abstr.*, *18*, 429-435, 1981.

Walsh, J. B., and M. A. Grosenbaugh, A new model for analyzing the effect of fractures on compressibility, *J. Geophys. Res.*, *84*, 3532-3536, 1979.

Wang, J. S. Y., T. N. Narasimhan, and C. H. Scholz, Aperture correlation of a fractal fracture, *J. Geophys. Res.*, *93*, 2216-2224, 1988.

Whitehouse, D. J., and J. F. Archard, The properties of ran-

dom surfaces of significance in their contact, *Proc. R. Soc. London, A, 316*, 97-121, 1970.

Yoshioka, N., and C. H. Scholz, Elastic properties of contacting surfaces under normal and shear loads, 1, Theory, *J. Geophys. Res.*, *94*, 17681-17690, 1989a.

Yoshioka, N., and C. H. Scholz, Elastic properties of contacting surfaces under normal and shear loads, 2, Comparison of theory with experiment, *J. Geophys. Res.*, *94*, 17691-17700, 1989b.

Zimmerman, R. W., D-W. Chen, and N. G. W. Cook, The effect of contact area on the permeability of fractures, *J. Hydrol.*, *139*, 79-96, 1992.

S. R. Brown, Geomechanics Department, Sandia National Laboratories, P.O. Box 5800, Albuquerque, NM 87185-0751. (email:srbrown@sandia.gov)

(Received January 21, 1994; revised December 2, 1994; accepted December 6, 1994.)